Journal of Materials Chemistry C

PAPER

View Article Online
View Journal | View Issue

Cite this: J. Mater. Chem. C, 2015, 3, 5033

Manipulations from oxygen partial pressure on the higher energy electronic transition and dielectric function of VO_2 films during a metal–insulator transition process

Peng Zhang,[a] Kai Jiang,[a] Qinglin Deng,[a] Qinghu You,[b] Jinzhong Zhang,[a] Jiada Wu,[b] Zhigao Hu*[a] and Junhao Chu[a]

Received 1st January 2015,
Accepted 13th April 2015

DOI: 10.1039/c5tc00002e

www.rsc.org/MaterialsC

Optical properties and metal–insulator transition (MIT) of vanadium dioxide (VO_2) films grown by pulsed laser deposition with different oxygen pressures (5 to 50 mTorr) have been investigated by temperature dependent transmittance spectra. Three interband critical points (E_1, E_2 and E_3) can be obtained *via* fitting transmittance spectra and the hysteresis behavior of the center transition energies E_1 and E_2 is presented. The VO_2 film grown at optimized oxygen pressure exhibits the well-defined resistivity drop ($\sim 10^3$ Ω cm) across the MIT process. It is found that the metal–insulator transition temperature (T_{MIT}) increases with the oxygen pressure and the complex dielectric functions are drastically affected by oxygen pressure. It is believed that the oxygen pressure can lead to lattice defects, which introduce the donor level and the acceptor level in the forbidden gap produced by oxygen vacancies and vanadium vacancies, respectively. The donor level provides electrons for higher empty π* bands, which can make the energy barrier lower and decrease critical temperature. On the contrary, electrons jumping from the $d_{||}$ band can be recombined by holes on the acceptor, impeding the MIT occurrence. It is claimed that the electronic orbital occupancy is closely related to oxygen pressure, which changes the energy barrier and manipulates the phase transition temperature. The present results are helpful to understand the fundamental mechanism of VO_2 films and practical applications for VO_2-based optoelectronic devices.

1 Introduction

The study of metal–insulator transition (MIT) in crystalline films is a subject of paramount importance, both from the fundamental point of view and its relevance to the transport properties of materials. One of the most extensively studied, because of its potential applications, is vanadium dioxide (VO_2), which undergoes a first-order metal–insulator transition at about 340 K with an abrupt increase in resistivity by several orders of magnitude.[1] The lattice in the metallic phase has the rutile structure ($P4_2/mn$), with the vanadium ions arranged in periodic chains parallel to the *c*-axis. In the insulating phase, the dimerization and the off-axis zigzag displacement of V–V pairs can result in a monoclinic structure ($P2_1/c$).[2–4] The origin of this MIT can be due to the formation of a Peierls state,[5] or it could be driven by Mott correlations,[6] or more likely it may have some mixed origin.[7,8] Therefore, the MIT region is intrinsically associated with structural and electronic band changes by strong coupling among the lattice, charge, spin and orbital occupancy.

Involving both electronic and lattice degrees of freedom, several factors are known to affect the metal–insulator transition temperature (T_{MIT}), such as doping,[9,10] stress[11,12] and oxygen vacancy.[13,14] Among them, oxygen vacancy has a tremendous effect on the characters of VO_2 films. Recently, optical properties of VO_2 films have been widely investigated.[15–18] Oxygen pressure tuning the band gap, T_{MIT}, and the effect of V–O stoichiometry on optical properties of VO_2 films have been reported.[19,20] It was believed that the increased oxygen content in vanadium oxide will reduce the magnitude of phase transition.[21] Despite the mechanism of oxygen partial pressure being extensively studied,[22,23] the fundamental mechanism for oxygen pressure modulated MIT process is still under debate. The influence of the oxygen pressure on the high energy transition and dielectric functions has been rarely studied. Moreover, most of the reports failed to reveal the internal mechanism of oxygen pressure in the electronic property that sets the energy scale for T_{MIT}. Therefore, interpreting the effect of oxygen pressure to tuning the MIT process of VO_2 film is critical for

[a] Key Laboratory of Polar Materials and Devices, Ministry of Education, Department of Electronic Engineering, East China Normal University, Shanghai 200241, China. E-mail: zghu@ee.ecnu.edu.cn; Fax: +86-21-54345119; Tel: +86-21-54345150
[b] Department of Optical Science and Engineering, Fudan University, Shanghai 200433, China

practical applications, such as Mott field-effect transistors and optical switches.[24,25]

In this article, the influences of different oxygen pressure on higher energy electronic transition and dielectric functions are presented. The abnormal electronic transition has been observed and can be interpreted by the orbital theory. Intrinsic evolution of oxygen pressure on modulating the MIT process through the hysteresis behavior of the transition energies is elucidated. The fundamental mechanism of the impurity level generated by oxygen vacancy and vanadium vacancy has been discussed in detail. It would be meaningful to clarify the relationship between the oxygen pressure and the absorption as well as dielectric function. Moreover, it is beneficial to grow high quality VO_2 films and develop potential applications.

2 Experimental section

2.1 Fabrication of VO_2 films

VO_2 films were prepared on a *c*-cut single crystal sapphire substrate using pulsed laser deposition (PLD). In order to obtain better crystalline quality, the substrates were rigorously cleaned in pure ethanol with an ultrasonic bath and were rinsed several times by de-ionized water before the deposition. The energy density of the laser beam at the target surface was maintained at 2 J cm^{-2} with a target-substrate distance of 6 cm. The VO_2 target was prepared from VO_2 powder (purity 99.95%). The vacuum chamber was evacuated down to 5×10^{-3} Pa. During the deposition oxygen gas was introduced into the chamber to maintain the desired pressure (5, 10, 20 and 50 mTorr). After deposition at room temperature (RT), amorphous films were annealed at 450 °C in nitrogen ambience by a thermal process for 1 h to obtain crystalline VO_2 films.

2.2 Microstructure, morphology, optical and electrical characterization of VO_2 films

From the measurement of scanning electron microscopy (SEM: Philips XL30FEG), the thickness of VO_2 films was estimated to be about 38, 41, 45 and 48 nm as the oxygen pressure increases. The structures of the VO_2 films were determined by X-ray diffraction (XRD) with Cu Kα radiation (λ = 0.1542 nm) at RT. The surface morphology of the VO_2 films was characterized by atomic force microscopy (AFM: Digital Instruments Icon, Bruker). X-ray photoelectron spectroscopy (XPS, AXIS Ultra^{DLD}, Japan) with Al Kα radiation ($h\nu$ = 1486.6 eV) was performed to investigate the valence state and the stoichiometry of the films. To characterize the electric properties across the phase transition boundary, we measured the resistance by a THMSE 600 heating/cooling stage (Linkam Scientific Instruments) in the temperature range from 20 °C to 100 °C. The silver (Ag) electrodes were welded at the surface of the VO_2 films and a short copper wire was connected to each of them. The normal-incident transmittance spectra at 25–90 °C were recorded using a double beam ultraviolet–infrared spectrophotometer (PerkinElmer Lambda 950) at the photon energy from 0.5 to 6.5 eV (190–2650 nm) with a spectral resolution of 2 nm. The VO_2 films on sapphire substrates were mount onto a heating stage (Bruker A599) for high temperature experiments.

3 Results and discussion

3.1 Structural analysis and electrical properties

The structures of the VO_2 films are shown in Fig. 1(a). Compared to the standard reference data (JCPDS No. 73-2362), the diffraction peak at about 2θ = 39.94° corresponds to a monoclinic VO_2 structure with the (200) preferred orientation for films grown at different oxygen pressure. Notably, the diffraction peak shows nearly a similar pattern, indicating that the strain should not be the main focus in the present study. It has been reported that the T_{MIT} of VO_2 film with a thickness of 13 nm deposited on the Al_2O_3 substrate is about 60 °C and the T_{MIT} increases with increasing thickness.[26] However, the T_{MIT} is only about 50 °C for the VO_2 film with a thickness of 38 nm grown at 5 mTorr in the present work. It suggests that the reduced T_{MIT} is caused by oxygen pressure instead of strain, even if the compressive strain exists. It is found that the thickness of the VO_2 films is relatively

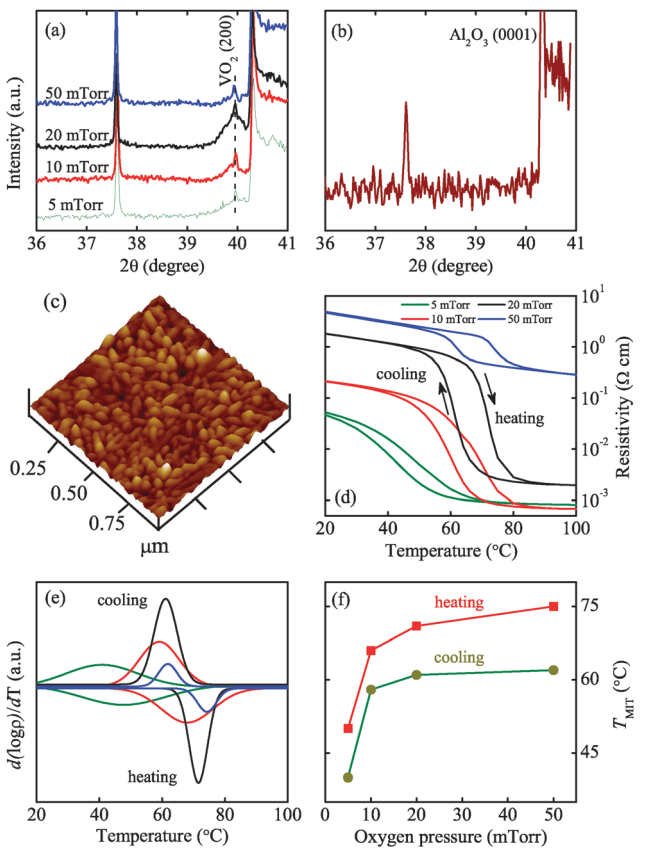

Fig. 1 (a) The XRD results for VO_2 films grown at different oxygen pressure. (b) The crystal orientation of the Al_2O_3 substrate. (c) AFM three-dimensional image for the film deposited at an oxygen pressure of 20 mTorr. The scale height is 20 nm and the measured area is 1×1 μm^2. (d) Temperature dependence of electrical resistivity for VO_2 films grown at various oxygen pressures. (e) Differential curves *versus* temperature during heating and cooling for the films. (f) Phase transition temperature as a function of oxygen pressure.

thin and the characteristic peak of the Al_2O_3 substrate is very strong. Therefore, the diffraction peak of VO_2 is weak compared to that from the Al_2O_3 substrate. In order to further affirm the characteristic peak of the VO_2 films, the peak of the Al_2O_3 substrate is shown in Fig. 1(b). Obviously, the peak at about $2\theta = 39.94^\circ$ can be derived from VO_2 films.

The surface microstructure of the VO_2 film grown at 20 mTorr is shown in Fig. 1(c). The size distribution of the grains varies from 40 nm to 75 nm. The root-mean-square roughness of the surface is only 1.7 nm, indicating the quite smooth surface morphology. Fig. 1(d) and (e) show temperature dependence of the electrical resistivity for VO_2 films grown at various oxygen deposition pressures together with differential curves. For the film grown at 5 mTorr, the transition occurs in a quite broad temperature range. However, VO_2 films grown at higher oxygen pressures (10 mTorr and 20 mTorr) exhibit a typical characteristic of the MIT process. Nevertheless, for the film grown at 50 mTorr, the resistivity curves display an unconspicuous change. It indicates that the quality of the films gradually exalts with oxygen pressure until 20 mTorr. It should be noticed that there may be some presence of higher valence vanadium oxide V_3O_7 due to excess oxygen in the film grown at 50 mTorr.[14] It suggests that the optimized VO_2 film grown at 20 mTorr exhibits the well-defined MIT characteristic. A three order magnitude of resistivity variation can be observed. The resistivity of the films grown at 5 mTorr and 10 mTorr maintains a small value of less than 10^{-3} Ω cm after MIT, while it is 10^{-3} Ω cm for the film grown at 20 mTorr. Obviously, the resistivity increasing with oxygen pressure is closely related to electron concentration at the metal state.[27]

From the differential curves in Fig. 1(e), the T_{MIT} increases with oxygen pressure. Phase transition temperature as a function of oxygen pressure is shown in Fig. 1(f). These results clearly indicate that the presence of oxygen vacancies induced by oxygen pressure modifies the MIT temperature and the magnitude of the resistivity drop effectively. The influence of energy barrier to MIT temperature can be taken into account.[28] It is believed that extra electrons induced by the oxygen vacancies can be localized at the empty π* band, decreasing the energy barrier. As a consequence, an earlier onset of MIT may be triggered.[29] The decreased oxygen content can make the concentration of oxygen vacancies increasing, which results in more electrons occupying the empty π* band. Then, electrons on π* band will form a weak conduction band and reduce the T_{MIT}. Therefore, the transition temperature increases with oxygen pressure.

3.2 NIR-UV transmittance spectra

The transmittance spectra from 25 °C to 80 °C during heating for VO_2 films are shown in Fig. 2. From the temperature dependence of infrared (IR) transmittance at selected incident photon energies ($h\nu = 0.47$ eV, $\lambda = 2600$ nm), the transmittance is 72.66%, 75.78%, 81.17% and 72.29% with increasing oxygen pressure at the insulating state. Ruzmetov *et al.* has reported that the variation of the mid-infrared reflectance at 0.4 eV is more than 60%, indicating excellent properties of the VO_2 film.[30]

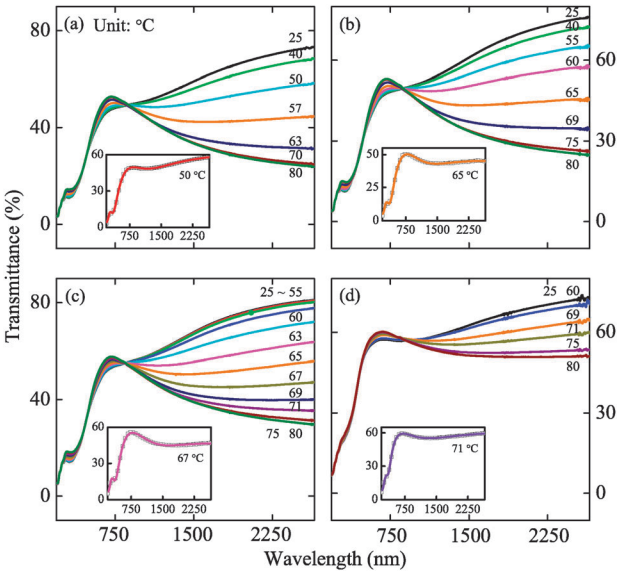

Fig. 2 The transmittance spectra for VO_2 films grown at (a) 5 mTorr, (b) 10 mTorr, (c) 20 mTorr and (d) 50 mTorr, respectively. The inset is the experimental (dotted lines) and best-fitted (solid lines) transmittance spectra of VO_2 films.

Compared to the change of the mid-infrared reflectance, the variation of transmittance at 0.47 eV is 49.1%, 51.2%, 52.0% and 21.6% with increasing oxygen pressure. One can see that the spectral change with the temperature occurs within 10 °C interval for film grown at 20 mTorr. However, the interval is about 25 °C and 20 °C for films grown at 5 mTorr and 10 mTorr, respectively. The results reveal the high optical performance for film grown at 20 mTorr. Note that even the interval is within 10 °C for film grown at 50 mTorr, optical properties of the film are inferior than other films. It is obvious that the oxygen pressure has great influence on optical properties and the MIT. Fig. 3(a) shows the hysteresis loops for temperature dependence of transmittance at the wavelength of 2600 nm for films grown at different oxygen pressures. For films grown at 5 mTorr, 10 mTorr and 20 mTorr, significant optical change can be observed. However, the change is smaller for the film grown at 50 mTorr (~22%) than those from other three films. From Fig. 3(b) and (c), optical switching and thermal hysteresis can be found in the near visible range (at 700 nm) and ultraviolet range (at 300 nm). Nevertheless, the variation is extremely small. Notably, the rotational direction of the hysteresis loop in the infrared range (2600–860 nm) is opposite to the visible-ultraviolet range (860–250 nm). These kinds of anomalous thermal hysteresis behaviors are closely related to the electronic transition.[31,32] Fig. 3(d) shows the corresponding transition of the three spectral region. In the infrared region, the V $3d_{\|}$ band overlaps the V $3d_{\|}$* band and electron concentration increases rapidly after MIT.[33] As a consequence, the variation of transmittance in the infrared region can be ascribed to the transition from the V $3d_{\|}$ band to the V $3d_{\|}$* band (E_1). In the near-visible region, a small reverse optical switching behavior can be observed. This is presumably associated with the

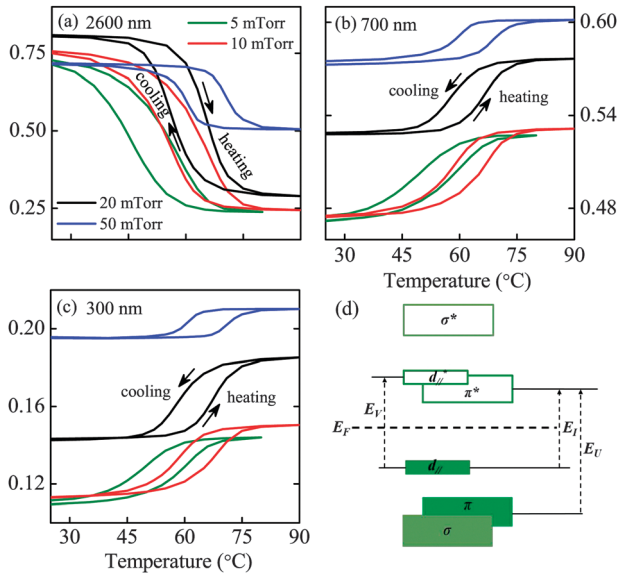

Fig. 3 Hysteresis loop of spectral transmittance at (a) 2600 nm (b) 700 nm (c) 300 nm as a function of temperature for VO_2 films. (d) The band scheme of three spectral region transitions.

transition from the filled V $3d_{\|}$ band to the empty V $3d_{\|}$* band (E_V). However, a subtle hysteresis loop appears in the ultraviolet range, which can be assigned to the higher electronic transition. It is the transition from the lower filled O 2p π band to the empty π* band (E_U).[34]

3.3 Optical properties and electronic structures

3.3.1 Theoretical calculation of transmittance. The inverse synthesis is based on a phenomenological model fitted to the experimental data. A three-phase layered structure (air/film/substrate) was used to calculate the UV-NIR transmittance of the VO_2 films.[35] The modeling spectra were constructed under the assumption that the films and the substrates are treated as isotropic materials. The optical component of each layer is expressed by a 2 × 2 matrix. Suppose the dielectric function of the film is ε, the vacuum is unity, and the substrate is ε_s. The resultant matrix M_r is described by the following product form

$$M_r = M_{vf}M_fM_{fs}. \quad (1)$$

Here, the interface matrix between the vacuum and film has the form

$$M_{vf} = \frac{1}{2\sqrt{\varepsilon}}\begin{bmatrix} \varepsilon+1 & \varepsilon-1 \\ \varepsilon-1 & \varepsilon+1 \end{bmatrix} \quad (2)$$

and the propagation matrix for the film is described by the equation

$$M_f = \begin{bmatrix} \exp\left(\frac{i2\pi\sqrt{\varepsilon}d}{\lambda}\right) & 0 \\ 0 & \exp\left(-\frac{i2\pi\sqrt{\varepsilon}d}{\lambda}\right) \end{bmatrix} \quad (3)$$

where λ is the incident wavelength and d is the thickness of the film. Correspondingly, the interface matrix between film and substrate is

$$M_{fs} = \frac{1}{2\sqrt{\varepsilon_s}}\begin{bmatrix} \sqrt{\varepsilon_s}+\sqrt{\varepsilon} & \sqrt{\varepsilon_s}-\sqrt{\varepsilon} \\ \sqrt{\varepsilon_s}-\sqrt{\varepsilon} & \sqrt{\varepsilon_s}+\sqrt{\varepsilon} \end{bmatrix}. \quad (4)$$

Thus, the transmittance T can be readily obtained from

$$T = \mathrm{Real}\left(\sqrt{\varepsilon}\right)\left|\frac{1}{M_{r1,1}}\right|^2. \quad (5)$$

The multireflections from the substrate are not considered in eqn (5). It should be emphasized that the absorption from the substrate must be taken into account to calculate the transmittance of the film-substrate system. The Drude–Lorentz (DL) oscillator dispersion relation is used to simulate the transmittance spectra, which can be written as follows[33]

$$\varepsilon(E) = \varepsilon_\infty - \frac{A_D}{E^2+iEB_D} + \sum_{k=1}^{3}\frac{A_k}{{E_k}^2-E^2-iEB_k} \quad (6)$$

where ε_∞ is the high-frequency dielectric constant. A_k, E_k, B_k and E is the amplitude, center energy, broadening of the jth oscillator and the incident photon energy, respectively. The parameter A_D is the square of the plasma frequency and B_D is the electron collision or damping frequency. The best-fitted transmittance spectra of VO_2 films on sapphire substrates are shown by the solid lines in Fig. 2. A good agreement can be observed, indicating that the dispersion model selected is reasonable.

3.3.2 Dielectric functions. The real part ε_1 and imaginary part ε_2 of the complex dielectric functions for VO_2 films grown at different oxygen pressures are given in Fig. 4(a)–(d), respectively. The imaginary part of the dielectric function ε_2 at the near infrared region increases drastically with the temperature, especially near the MIT range. It signals transition to the metallic phase. Particularly, it is found that the value of the ε_2 change ($\Delta\varepsilon_2$) from the insulator to the metal state decreases gradually below ~1.5 eV as well as the ε_1 change ($\Delta\varepsilon_1$) with increasing oxygen pressure. The $\Delta\varepsilon_2$ is 21, 19, 14 and 5 for films grown at 5 mTorr, 10 mTorr, 20 mTorr and 50 mTorr, respectively. Correspondingly, the $\Delta\varepsilon_1$ is 14, 13, 12 and 4, respectively. It is believed that the variation of ε_2 in the near-infrared region is closely related to the electrical properties such as carrier concentration or conductivity.[27] The carrier concentration is proportional to the square of the plasma frequency A_D. At low temperature, the values of A_D are extremely small, suggesting an insulator behavior. At the metal state, A_D is 5.119, 5.116, 4.154 and 2.959 eV for films grown at 5 mTorr, 10 mTorr, 20 mTorr and 50 mTorr, respectively. It is found that A_D decreases with the oxygen pressure, indicating that the carrier concentration decreases with the oxygen pressure on the condition of unity electron average effective mass.[36] Therefore, the variation of $\Delta\varepsilon_2$ at the near-infrared region can be ascribed to the change of carrier concentration. It also illustrates that oxygen vacancies are able to trap extra electrons on the empty π* band, which can increase the carrier concentration.

3.3.3 Defect behaviors. Fig. 5(a) displays the overall core level XPS survey spectra of the VO_2 film grown at the oxygen

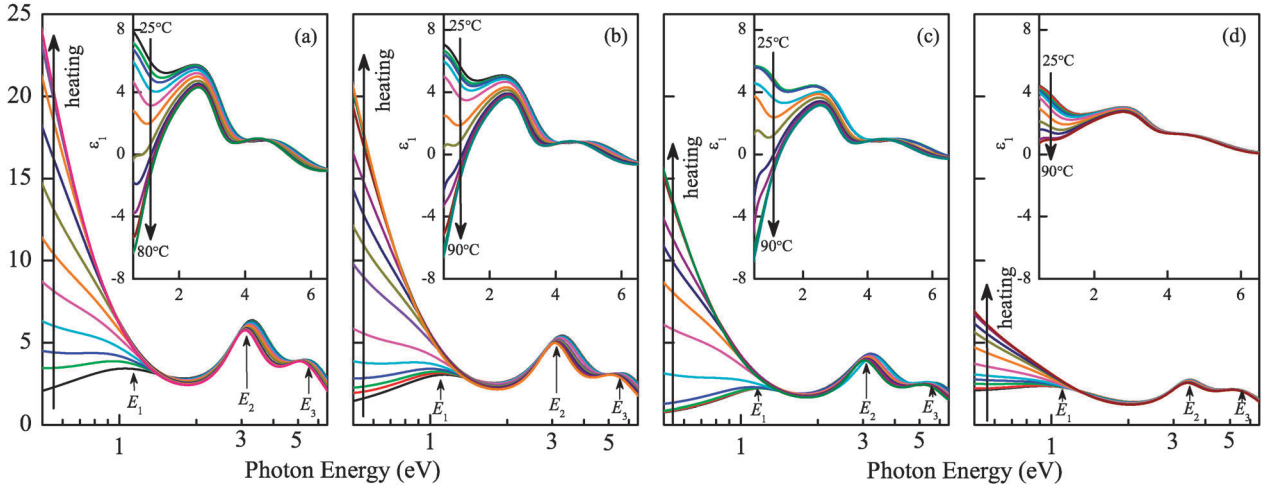

Fig. 4 The real ε_1 (inset) and imaginary ε_2 parts of the complex dielectric functions for VO_2 films deposited at (a) 5 mTorr, (b) 10 mTorr, (c) 20 mTorr and (d) 50 mTorr, respectively. Three interband transition features are indicated by the arrows. Note that the horizontal coordinate of ε_2 is the logarithmic unit to enlarge the transparent region.

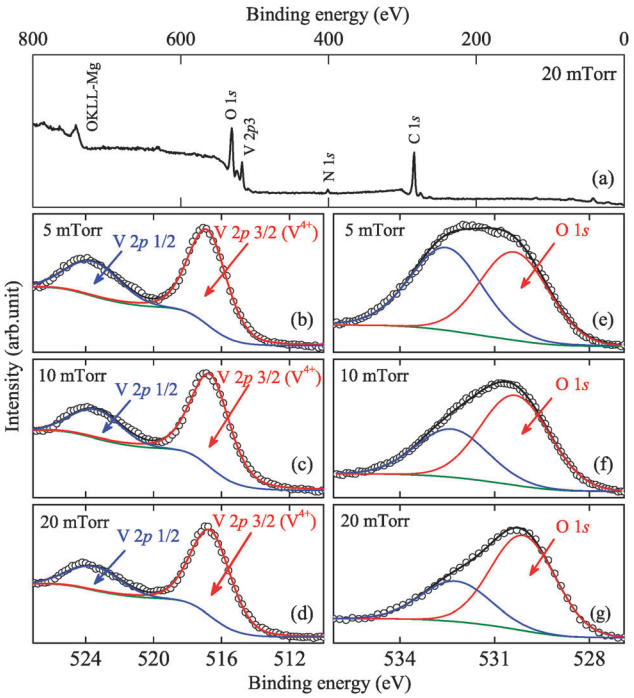

Fig. 5 (a) Overall core level XPS spectra for the VO_2 film grown at 20 mTorr. (b)–(d) XPS spectra of V 2p lines with the Lorentzian–Gaussian dividing peak analysis for the VO_2 films grown at an oxygen pressure of 5 mTorr, 10 mTorr and 20 mTorr, respectively. (e)–(g) XPS spectra of O 1s lines with the Lorentzian–Gaussian dividing peak analysis for the VO_2 films grown at an oxygen pressure of 5 mTorr, 10 mTorr and 20 mTorr, respectively. The solid lines represent the nonlinear fitting results.

pressure of 20 mTorr. The intense peaks of V 2p and O 1s can be observed. Fig. 5(b)–(g) show the Lorentzian–Gaussian dividing peak analysis of V 2p and O 1s peaks for three films grown at 5 mTorr, 10 mTorr and 20 mTorr, respectively. The 1/2 and 3/2 spin–orbit doublet components of the V 2p photoelectron are found to be located at about 523.8 eV and 516.7 eV, respectively.[37] The peaks located at about 516.7 eV can be assigned to V^{4+}. It is consistent with the XPS analysis reported previously.[38–40] Notably, the present films were annealed at nitrogen ambience, which is helpful to prevent the formation of the V^{5+} valence state. It is found that the films can be easily turned into V_2O_5 during annealing at oxygen ambience. Although the XPS measurement can reflect the information from the topmost layers instead of the entire film, it can be seen that the present results are similar to the bulk regions, where the V^{4+} peak is located at about 516.5 eV.[40] It may be attributed to the preparation conditions of the present work. From the V 2p peaks, we cannot distinguish the existence of V^{5+} or V^{3+}. Through the hard X-ray photoelectron spectroscopy (HAXPES) and surface XPS spectra, V^{5+} or V^{4+} can be distinguished by the shoulder peak.[41] In addition, the shoulder peak of V^{5+} can be also observed in the previous report.[42] However, the shoulder peak of V^{5+} or V^{3+} cannot be observed in the present XPS spectra, indicating that the content of the V^{5+} or V^{3+} is low and can be ignored. On the contrary, the shoulder peak of the surface adsorption oxygen or hydroxyl contributions can be obviously observed from the O 1s spectra. The main peak located at about 530 eV can be assigned to O 1s. The shoulder peak located at about 532 eV should be attributed to the surface adsorption oxygen. Therefore, the effect of surface adsorption oxygen should be excluded while calculating the V : O ratios.

Through quantitative analysis of XPS results, the stoichiometry is $VO_{1.895}$, $VO_{1.963}$ and $VO_{2.042}$ for films grown at 5 mTorr, 10 mTorr and 20 mTorr, respectively. It is obvious that oxygen vacancies exist in films grown at 5 mTorr and 10 mTorr. Moreover, the concentration of oxygen vacancies decreases with oxygen pressure and disappears with the O/V ratio exceeding 2. For films grown at 20 mTorr, the stoichiometry indicates that oxygen is in excess or vanadium sites are vacant in the film. Nevertheless, the deviation is subtle for films grown at 10 mTorr and 20 mTorr. However, the T_{MIT} is lower than that of the bulk VO_2 for oxygen deficiency of $VO_{1.963}$ film. On the contrary, the T_{MIT} is higher than 68 °C for oxygen excess of $VO_{2.042}$ film. The variation of the

T_{MIT} indicates that the VO_2 film is quite sensitive to oxygen stoichiometry. The phenomenon further demonstrates that an earlier onset of MIT can be triggered by oxygen vacancies. Goodenough has proposed that nonstoichiometric $VO_{2+\varepsilon}$ ($0.00 \leq \varepsilon \leq 0.07$) does not contain π^* electrons at $T \leq T_{MIT}$ to depress the transition temperature.[43] That is to say, the transition temperature can be reduced if the π^* band was occupied by electrons at $T \leq T_{MIT}$. Therefore, it demonstrates that delocalization electrons can be trapped at the π^* band to depress the T_{MIT} owing to the existence of oxygen vacancies.

3.3.4 Electronic transition and band structure analysis. Three features can be identified from the ε_2 curves, which are labeled with E_1, E_2, and E_3, respectively. Several singularities denote the corresponding electronic transition between the filled and empty bands. At RT, the transition energies assigned from the ε_2 can be located at ~1.22, ~3.37 and ~5.90 eV for the VO_2 films. Compared to the reflectivity spectrum for VO_2 film at RT,[44] the singularities in ε_2 at 1.32, 3.60 and 5.89 eV are assigned to specific interband transitions. The three transitions can be assigned to the following electronic transitions:[45] (i) lower V 3d filled $d_{\parallel}$ band to the empty π^* band; (ii) the filled O 2p π band to the empty π^* band; (iii) lower V 3d filled $d_{\parallel}$ band to the empty σ^* band. Fig. 6(a) and (b) show temperature dependent interband transition energies E_1 and E_2, respectively. The change of the transition energies is closely related to the transformation of the band gap, especially for E_1 transition. In the metal phase, the band gap becomes zero due to the $d_{\parallel}$ band overlapping the π^* band,[41] which can be reflected by high mid-infrared absorption changes in reflectance[30] and transmittance experiment. According to the Goodenough orbital theory,[43] the fundamental band gap can be obtained by $E_v - E_c$, where E_v and E_c is the bottom of the valence band of the π^* band and the top of the conduction band of bonding the $d_{\parallel}$ band, respectively.

It is worth noting that the E_1 is the transition from the $d_{\parallel}$ band to the π^* band as well. Therefore, it is understandable that E_1 will disappear with the overlapping of the $d_{\parallel}$ band and the π^* band at the metal state. However, E_1 still appears with smaller energy at the metal state. From the imaginary part of dielectric functions, it can be observed that the E_1 peak disappears gradually with increasing temperature. It is difficult to identify the subtle transition of the E_1 at the metal state. It likely illustrates that the subtle energy is not caused by the transition from the occupied $d_{\parallel}$ center to the unoccupied π^* center. H. Kakiuchida *et al.*[46] has observed that the E_1 transition is absent at the metal state for the stoichiometric VO_2 film. Therefore, it is obvious that the subtle energy is not caused by the transition from the occupied $d_{\parallel}$ center to the unoccupied π^* center. For the non-stoichiometric VO_2 films, the subtle energy of E_1 can be assigned to the role of defects at the metal state. Thus, it is most likely that the E_1 transition is due to the existence of impurity level at the metal state. Donor-like and acceptor-like states have been reported by Berglund *et al.*[47] It is believed that the energy gap is likely filled by donor-like and acceptor-like states, the charge density of which may be larger than the associated carriers in the band. It was reported that the acceptor level and donor level are located in the fundamental band gap.[42] Moreover, Thimsen *et al.* believed that surface defects can trap electrons in nanomaterials and an electron acceptor trap on the surface limits the conductivity.[48] It is in good agreement with the resistivity of the films at the metal state. Based on the abnormal transition of the E_1 at the metal state, it indicates that there is the energy level lying between the π band and the π^* band, which transfers electrons to the π^* band.

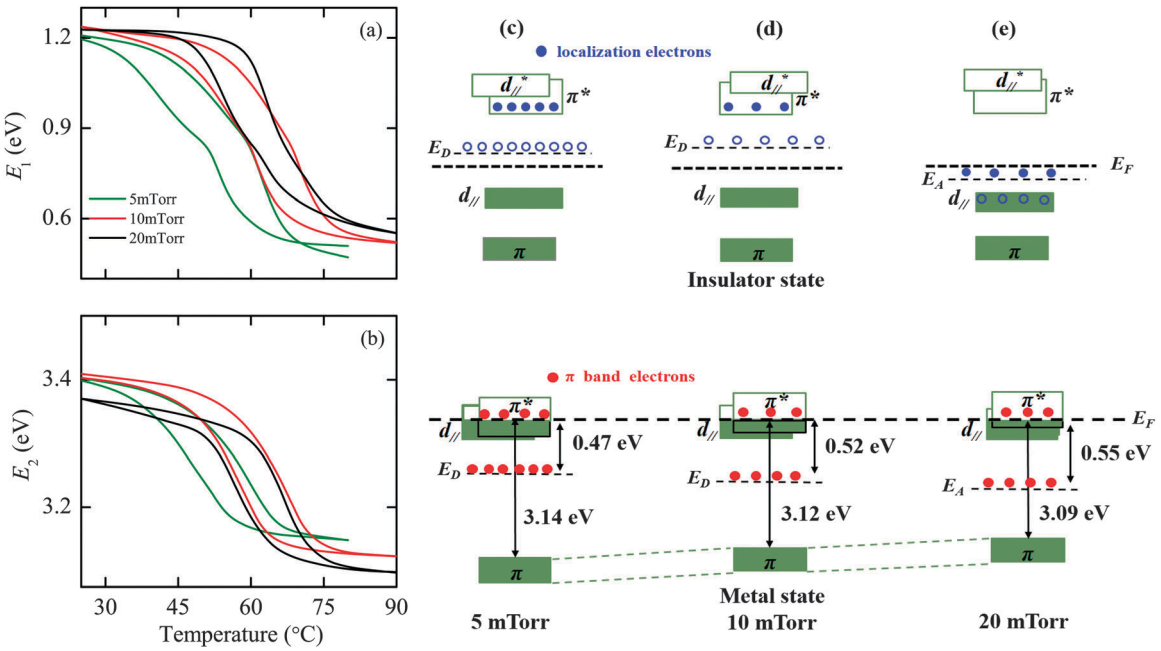

Fig. 6 The hysteresis loop of the electronic transition (a) E_1 and (b) E_2 for the VO_2 film grown at different oxygen pressure. The band scheme for VO_2 films grown at (c) 5 mTorr, (d) 10 mTorr and (e) 20 mTorr in the insulator state and the metal state, respectively.

At the insulator state, the values of E_1 are 1.20, 1.23 and 1.22 eV and the values of E_2 are 3.40, 3.40 and 3.37 eV for the films grown at 5 mTorr, 10 mTorr and 20 mTorr, respectively. It illustrates that the transition energies E_1 and E_2 are almost undisturbed by oxygen pressure. At the metal state, it is obvious that the transition energy E_1 still exists and becomes higher with increasing oxygen pressure. The corresponding value is 0.47, 0.52 and 0.55 eV, respectively. With increasing oxygen pressure, the transition energy E_2 is 3.14, 3.12 and 3.09 eV, respectively. It can be believed that the abnormal phenomenon is closely related to the donor level (E_D) and acceptor level (E_A).[42] The band scheme for VO_2 was presented to illustrate the location of E_D and E_A in Fig. 6(c)–(e). Based on the nonstoichiometric VO_2 and the abnormal transition, the E_D and E_A are generated by oxygen vacancies and vanadium vacancies, respectively. It is believed that the π^* band can be occupied by more electrons, which are transfered from the $d_{\parallel}$ band due to the strain at the film interface. Then, the MIT can be decreased.[49] Oxygen vacancies are able to localize extra electrons at the empty π^* band. As a result, the thermal energy barrier for phase transition can be reduced.[50] Therefore, electrons that E_D offers to the empty π^* band make the energy barrier decreasing as well as the T_{MIT}. For a film grown at 5 mTorr, E_D is the nearest to the Fermi level (E_F) and extra electron concentration induced by oxygen vacancies is the largest. Extra electrons are located on E_D and ionized at RT, leaving holes on E_D. Then, the ionized electrons transfer to the empty π^* band, forming a weak conduction band. The energy barrier is reduced and an earlier onset of MIT can be triggered. For film grown at 10 mTorr, E_D is far away from E_F. Thus, extra electron concentration is less than that for the film grown at 5 mTorr. Therefore, T_{MIT} for film grown at 10 mTorr (66 °C) is higher than the value for the film grown at 5 mTorr (50 °C). However, the T_{MIT} is 71 °C for film grown at 20 mTorr. Holes on E_A generated by vanadium vacancies may be recombined by electrons on the $d_{\parallel}$ band, lifting the energy barrier and hindering the occurrence of MIT.

On the basis of the crystal field model,[43,51] the structural transition and electronic band variation are closely associated with hybridization of the O 2p orbitals with V 3d orbitals (p–d hybridization). During the MIT process, the dimerization of the V ions will be paired along the *c* axis, which makes the bonding $d_{\parallel}$ band overlapping with the antibonding $d_{\parallel}^*$ band across the E_F and down-shifts the π^* band. In addition, the paired V–V ions decrease the p–d overlapping and reduce the hybridization, making the highly directional $d_{\parallel}$ orbital and π^* orbital partially occupied. It is clear that the MIT process contains the structure variation as well as the electronic band change. Thus, the energy band near E_F is closely associated with the crystal structure. Therefore, the donor level most likely down-shifts below E_F according to the value of E_1 after MIT. At the metal state, the position of E_D and E_A has been shown in the band scheme. Notably, the E_D level will be occupied by electrons, which are transfered from the π band after MIT. However, electrons on E_D and E_A are located in the unstable state, which will jump to π^* again and reach the equilibrium state at last due to thermal excitation. Thus, E_1 still keeps subtle energy after MIT. Nevertheless, the electrons contributing to the π^* band are few and the impact can be ignored. The conquered energy barrier increases with oxygen pressure during the MIT, which makes the impurity level further away from E_F. In addition, the π band likely shifts up with oxygen pressure.[12,49] Therefore, E_1 energy gradually increases while E_2 energy declines. It is well understood that the variation of E_1 and E_2 is attributed to the impurity level at the metal state. The suppression of the MIT is derived from the oxygen vacancy. Therefore, the oxygen pressure plays an important role in optical properties, electrical properties, and phase transition.

4 Conclusion

To summarize, the influences of the oxygen pressure on E_1 and E_2, and real ε_1 and imaginary ε_2 parts of the complex dielectric functions have been investigated by temperature dependent transmittance spectra. The possible fundamental mechanism of the impurity level during the MIT process is discussed in detail. It is believed that energy scale for the MIT can be set and the critical temperature can be adjusted through regulating orbital occupancy. Therefore, the present data should be helpful to reveal the relationships between the oxygen pressure and the modulated MIT process.

Acknowledgements

One of the authors (P. Zhang) would like to thank Dr Z. H. Duan for constructive discussions. This work was financially supported by Major State Basic Research Development Program of China (Grant No. 2011CB922200 and 2013CB922300), the Natural Science Foundation of China (Grant No. 11374097 and 61376129), Projects of Science and Technology Commission of Shanghai Municipality (Grant No. 14XD1401500, 13JC1402100, and 13JC1404200), and the Program for Professor of Special Appointment (Eastern Scholar) at Shanghai Institutions of Higher Learning.

References

1 F. J. Morin, *Phys. Rev. Lett.*, 1959, **3**, 34–36.
2 J. Wei, Z. H. Wang, W. Chen and D. H. Cobden, *Nat. Nanotechnol.*, 2009, **4**, 420–424.
3 V. Pardo and W. E. Pickett, *Phys. Rev. Lett.*, 2009, **102**, 166803.
4 P. Baum, D. S. Yang and A. H. Zewail, *Science*, 2007, **318**, 788–792.
5 R. M. Wentzcovitch, W. W. Schulz and P. B. Allen, *Phys. Rev. Lett.*, 1994, **72**, 3389–3392.
6 T. M. Rice, H. Launois and J. P. Pouget, *Phys. Rev. Lett.*, 1994, **73**, 3042.
7 S. Biermann, A. Poteryaev, A. I. Lichtenstein and A. Georges, *Phys. Rev. Lett.*, 2005, **94**, 026404.
8 V. R. Morrison, R. P. Chatelain, K. L. Tiwari, A. Hendaoui, A. Bruhacs, M. Chaker and B. J. Siwick, *Science*, 2014, **346**, 445–448.

9 T. L. Wu, L. Whittaker, S. Banerjee and G. Sambandamurthy, *Phys. Rev. B: Condens. Matter Mater. Phys.*, 2011, **83**, 073101.
10 H. Takami, T. Kanki, S. Ueda, K. Kobayashi and H. Tanaka, *Phys. Rev. B: Condens. Matter Mater. Phys.*, 2012, **85**, 205111.
11 W. T. Liu, J. Cao, W. Fan, Z. Hao, M. C. Martin, Y. R. Shen, J. Wu and F. Wang, *Nano Lett.*, 2011, **11**, 466–470.
12 N. B. Aetukuri, A. X. Gray, M. Drouard, C. Matteo, L. Gao, A. H. Reid, R. Kukreja, H. Ohldag, C. A. Jenkins, E. Arenholz, K. P. Roche, H. A. Dörr, M. G. Samant and S. S. P. Parkin, *Nat. Phys.*, 2013, **9**, 661–666.
13 J. Jeong, N. Aetukuri, T. Graf, D. Schladt, M. G. Samant and S. S. P. Parkin, *Science*, 2013, **339**, 1402–1405.
14 H. Kim, N. Charipar, M. Osofsky, S. B. Qadri and A. Pique, *Appl. Phys. Lett.*, 2014, **104**, 081913.
15 M. Nazari, Y. Zhao, V. V. Kuryatkov, Z. Y. Fan, A. A. Bernussi and M. Holtz, *Phys. Rev. B: Condens. Matter Mater. Phys.*, 2013, **87**, 035142.
16 J. M. Atkin, S. Berweger, E. K. Chavez and M. B. Raschke, *Phys. Rev. B: Condens. Matter Mater. Phys.*, 2012, **85**, 020101.
17 S. Lysenko, V. Vikhnin, A. Rua, F. Fernandez and H. Liu, *Phys. Rev. B: Condens. Matter Mater. Phys.*, 2010, **82**, 205425.
18 W. W. Li, J. J. Zhu, J. R. Liang, Z. G. Hu, J. Liu, H. D. Chen and J. H. Chu, *J. Phys. Chem. C*, 2011, **115**, 23558–23563.
19 Q. Yu, W. W. Li, J. R. Liang, Z. H. Duan, Z. G. Hu, J. Liu, H. D. Chen and J. H. Chu, *J. Phys. D: Appl. Phys.*, 2013, **46**, 055310.
20 S. X. Zhang, I. S. Kim and L. J. Lauhon, *Nano Lett.*, 2011, **11**, 1443–1447.
21 H. W. Liu, L. M. Wong, S. J. Wang, S. H. Tang and X. H. Zhang, *Appl. Phys. Lett.*, 2013, **103**, 151908.
22 M. Nazari, C. Chen, A. A. Bernussi, Z. Y. Fan and M. Holtz, *Appl. Phys. Lett.*, 2011, **99**, 071902.
23 S. Kittiwatanakul, J. Laverock, D. N. Jr, K. E. Smith, S. A. Wolf and J. W. Lu, *J. Appl. Phys.*, 2013, **114**, 053703.
24 Z. Yang, C. Ko and S. Ramanathan, *Annu. Rev. Mater. Res.*, 2011, **41**, 337–367.
25 A. Cavalleri, C. Toth, C. W. Siders, J. A. Squier, F. Raksi, P. Forget and J. C. Kieffer, *Phys. Rev. Lett.*, 2001, **87**, 237401.
26 S. Kittiwatanakul, S. A. Wolf and J. W. Lu, *Appl. Phys. Lett.*, 2014, **105**, 073112.
27 D. Ruzmetov, S. D. Senanayake, V. Narayanamurti and S. Ramanathan, *Phys. Rev. B: Condens. Matter Mater. Phys.*, 2008, **77**, 195442.
28 R. Lopez, T. E. Haynes and L. A. Boatner, *Phys. Rev. B: Condens. Matter Mater. Phys.*, 2002, **65**, 224113.
29 L. L. Fan, S. Chen, Y. F. Wu, F. H. Chen, W. S. Chu, X. Chen, C. W. Zou and Z. Y. Wu, *Appl. Phys. Lett.*, 2013, **103**, 131914.
30 D. Ruzmetov, K. T Zawilski, S. D Senanayake, V. Narayanamurti and S. Ramanathan, *J. Phys.: Condens. Matter*, 2008, **20**, 465204.
31 J. Li and J. Dho, *Appl. Phys. Lett.*, 2011, **99**, 231909.
32 J. Dho, W. S. Kim and N. H. Hur, *Phys. Rev. Lett.*, 2001, **87**, 187201.
33 W. W. Li, Q. Yu, J. R. Liang, K. Jiang, Z. G. Hu, J. Liu, H. D. Chen and J. H. Chu, *Appl. Phys. Lett.*, 2011, **99**, 241903.
34 W. W. Li, J. J. Zhu, X. F. Xu, K. Jiang, Z. G. Hu, M. Zhu and J. H. Chu, *J. Appl. Phys.*, 2011, **114**, 053703.
35 Z. G. Hu, M. B. M. Rinzan, S. G. Matsik, A. G. U. Perera, G. V. Winckel, A. Stintz and S. Krishna, *J. Appl. Phys.*, 2005, **97**, 093529.
36 K. Okazaki, H. Wadati, A. Fujimori, M. Onoda, Y. Muraoka and Z. Hiroi, *Phys. Rev. B: Condens. Matter Mater. Phys.*, 2004, **69**, 165104.
37 Z. T. Zhang, Y. F. Gao, Z. Chen, J. Du, C. X. Cao, L. T. Kang and H. J. Luo, *Langmuir*, 2010, **26**, 10738.
38 G. Gopalakrishnan and S. Ramanathan, *J. Mater. Sci.*, 2011, **46**, 5768–5774.
39 D. H. Youn, H. T. Kim, B. G. Chae, Y. J. Hwang, J. W. Lee, S. L. Maeng and K. Y. Kang, *J. Vac. Sci. Technol., A*, 2004, **22**, 719–724.
40 Y. J. Cui, X. W. Wang, Y. Zhou, R. Gordon and S. Ramanathan, *J. Cryst. Growth*, 2012, **338**, 96–102.
41 N. F. Quackenbush, J. W. Tashman, J. A. Mundy, S. Sallis, H. Paik, R. Misra, J. A. Moyer, J. H. Guo, D. A. Fischer, J. C. Woicik, D. A. Muller, D. G. Schlom and L. F. J. Piper, *Nano Lett.*, 2013, **13**, 4857–4861.
42 C. H. Chen and Z. Y. Fan, *Appl. Phys. Lett.*, 2009, **95**, 262106.
43 J. B. Goodenough, *J. Solid State Chem.*, 1971, **3**, 490–500.
44 G. Anibal and C. Y. K. Clarence, *Phys. Rev. B: Condens. Matter Mater. Phys.*, 1971, **5**, 3138–3143.
45 M. M. Qazilbash, A. A. Schafgans, K. S. Burch, S. J. Yun, B. G. Chae, B. J. Kim, H. T. Kim and D. N. Basov, *Phys. Rev. B: Condens. Matter Mater. Phys.*, 2008, **77**, 115121.
46 H. Kakiuchida, P. Jin, S. Nakao and M. Tazawa, *Jpn. J. Appl. Phys.*, 2007, **46**, L113.
47 C. N. Berglund and H. J. Guggenheim, *Phys. Rev.*, 1969, **185**, 1022–1033.
48 E. Thimsen, M. Johnson, X. Zhang, A. J. Wagner, K. A. Mkhoyan, U. R. Kortshagen and E. S. Aydil, *Nat. Commun.*, 2014, **5**, 5822.
49 L. L. Fan, S. Chen, Z. L. Luo, Q. H. Liu, Y. F. Wu, L. Song, D. X. Ji, P. Wang, W. S. Chu, C. Gao, C. W. Zou and Z. Y. Wu, *Nano Lett.*, 2014, **14**, 4036–4043.
50 X. G. Tan, T. Yao, R. Long, Z. H. Sun, Y. G. Feng, H. Cheng, X. Yuan, W. Q. Zhang, Q. H. Liu, C. Z. Wu, Y. Xie and S. Q. Wei, *Sci. Rep.*, 2012, **2**, 466.
51 J. B. Goodenough, *Phys. Rev.*, 1960, **117**, 1442–1451.

